Classification of multiple diseases based on wavelet features

Nalini Bodasingi, Narayanam Balaji

Department of ECE, JNTUK University College of Engineering, Vizianagaram, Andhra Pradesh 535003, India
E-mail: nalinib.ece@jntukucev.ac.in

Published in *The Journal of Engineering*; Received on 7th June 2016; Accepted on 11th January 2017

Abstract: This study presents an efficient disease classification approach based on medical images. The approach is more efficient as it reduces the computational complexity. The implementation uses only two wavelet filters in selecting the texture features as compared with five filters used in the earlier research works. The computed average and energy features are fed to feed-forward neural network (FFNN) and support vector machine (SVM) classifiers. The SVM is proved as a better classifier than the FFNN for all the three diseases related to skin, breast and retina with an improved accuracies of 89%, 92% and 100%, respectively. Also, a graphical user interface is developed useful for various disease classification based on the whole dataset of size 100.

1 Introduction

Medical imaging plays an important role as a diagnostic tool in all medical applications. The medical images are produced at an exponential rate every day creating a huge database for analysis. In the diagnosis of a complex disease, these medical images consist of important and huge information related to shape, colour and texture. Breast cancer is an almost common cancer in women with millions of cases increasing every year worldwide. Mammograms are the imaging modality that uses a lower radiation dose for diagnosing breast cancer [1]. The incidences of skin cancer have been increasing for the past decade for both non-melanoma and malignant melanoma cases. The most pigmented skin lesion (PSL) images are obtained by non-invasive techniques such as dermatological photographs (clinical images) and dermoscopy used for the diagnosis of the PSLs used in computer-aided diagnosis [2]. These clinical images are RGB images and with high resolutions, which are widely used by the dermatologists for skin cancer diagnosis. In the global blindness statistics, glaucoma is the main cause with the severity of visual loss. There are many testing methods for glaucoma such as perimetry, tonometry and ophthalmoscopy/funduscopy. The retinal fundus image is a dilated eye examine which shows the shape and colour of the optic nerve, fovea and the blood vessels. These images are all RGB images. Development of an efficient approach for classifying these diseases with accuracy will help the clinician for proper diagnosis hence an effort is made for the development of a graphical user interface (GUI) based disease classification approach.

This paper is organised as follows. Section 2 describes the background of the related work, Section 3 presents the details of dataset, Section 4 presents methodology of the proposed model, Section 5 demonstrates the performance metrics, Section 6 shows experimental results, comparative analysis and discussion, and the final section presents conclusions and future work.

2 Related work

The literature survey indicates that the content-based image retrieval systems are useful for clinicians to improve their accuracy. The physician can arrive at a particular decision about the disease by observing similar cases of patients which will benefit both physician and the system. There are several methods employed for the analysis in the classification of digitalised biomedical images like skin cancer [3, 4], breast cancer [5–7] and retinal images [8–10]. For extracting significant texture features, various texture classification methods like statistical, geometrical and signal processing types can be used. Texture analysis has played a major role in the characterisation of biomedical images. This analysis can be utilised for much disease diagnosis, especially breast cancer, skin and retina for feature extraction and subsequent classification. Dong and Wang [5] obtained a classification rate of 80% while using Gabor filter banks and KNN classifier. The use of the dual-tree complex wavelet transform and support vector machine (SVM) employed in [6] classifies the benign and malignant images with an accuracy of 86.64%. For diagnosis of retinal disease such as glaucoma detection, many studies have been made for its automatic classification. Automated clinical decision support systems in ophthalmology, such as CASNET/glaucoma [11, 12], which are designed for decision support system was developed for disease identification in the eye. The use of texture features and higher order spectra (HOS) features were proposed by Acharya *et al.* [13] for glaucomatous image classification in which HOS derives amplitude and phase information while texture provides measures such as smoothness, coarseness and regularity. The experimental results show 90% classification accuracy by using SVM. In [10], the authors used five wavelet filters to obtain the wavelet-based feature for classification of glaucoma. In the problem of skin-related digital image classification, the skin lesions are evaluated using 'ABCD' features which include asymmetry, border irregularity, colour variation and spanned diameter. For skin cancer diagnosis this ABCD rule was used, where the A, B and C features analyse the texture information. The classification of medical images was analysed using SVM [14]. Manousaki *et al.* [15] used the colour parameter with geometrical and texture parameter which resulted in 69% sensitivity. The texture analysis approach measures texture features such as skewness, kurtosis, entropy, homogeneity at the different level of wavelets. The approach develops feature vectors which are used to classify lesions using the machine-learning algorithms [16, 17]. In this work, the disease diagnosis is based on the wavelet texture features. These texture features are obtained by employing two wavelet filters for the purpose of classification of normal and abnormal images related to the diseases with better accuracy.

3 Dataset

In the implemented approach, three different disease-related datasets of breast, skin and retina are considered. The datasets used are obtained from standard databases for classification. A total of 100 digital mammogram images consisting of 50 normal and 50 abnormal images are considered from the Digital Database for Screening Mammography [18]. For retina, the 100 retinal fundus

images are used in this work, and these standard images are from the DRIVE [19] and STATRE [20] database, out of which 50 normal and 50 glucomatous images. Finally, a dataset of 100 skin images is collected from the available Internet resources for the classification purpose. The dataset consists of 50 malignant melanoma images taken from the DanDerm web resource [21], and the other 50 are the non-melanoma skin images taken from the DermNetNz source [22]. All of the images in the each of the three datasets are made with a resolution of 512×512 pixels and stored in lossless JPEG format. The number of biomedical images used across each dataset is constant. These are used for binary classification of normal and abnormal images. Figs. 1–3 illustrate the normal and abnormal examples for mammograms, skin and retina images respectively.

4 Methodology

The overall process employed in the proposed work is depicted as follows. In the proposed work of multiple disease diagnosis, a total of 30 images for each of mammograms, skin and retina datasets are considered, of which 15 are normal and other 15 are abnormal images which are used for classification of images for each category. Initially, the biomedical images in the three datasets are first preprocessed by subjecting them to the standard histogram equalisation. Then, the discrete wavelet transform (DWT) is applied to the processed image to obtain the detail coefficients consisting of high-frequency image components that are taken and for which the single-valued statistical filter wavelet features are computed. From these extracted features, the required wavelet features are selected based on the *p*-value method. Finally, the feature vectors are fed to the feed-forward neural network (FFNN) and SVM classifiers for the disease diagnosis. The flow diagram of disease classification approach is shown in Fig. 4, and this method is further explained in detail in the following sections.

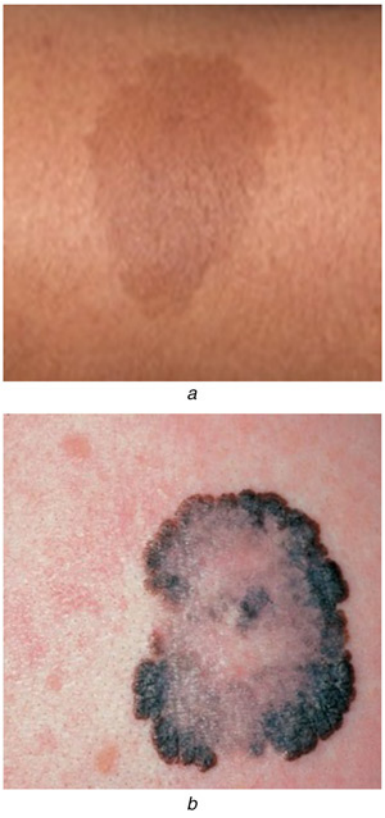

Fig. 2 *Examples of skin images*
a Non-melanoma
b Malignant melanoma

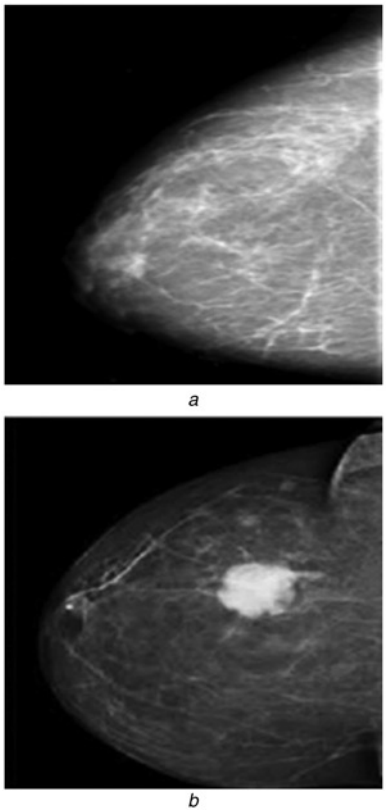

Fig. 1 *Examples of mammogram images*
a Normal
b Abnormal

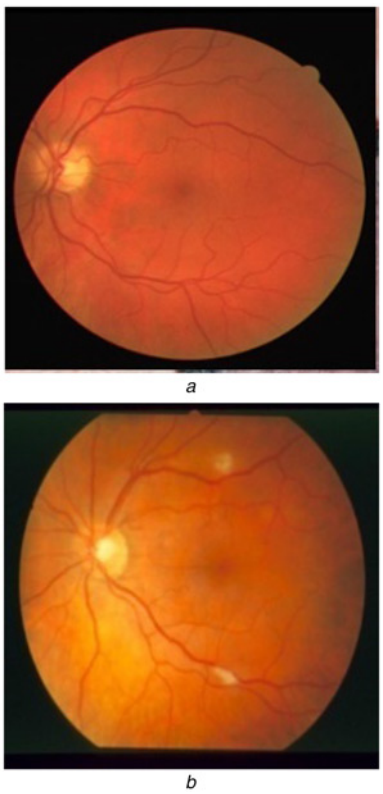

Fig. 3 *Examples of retinal fundus images*
a Normal
b Glaucoma

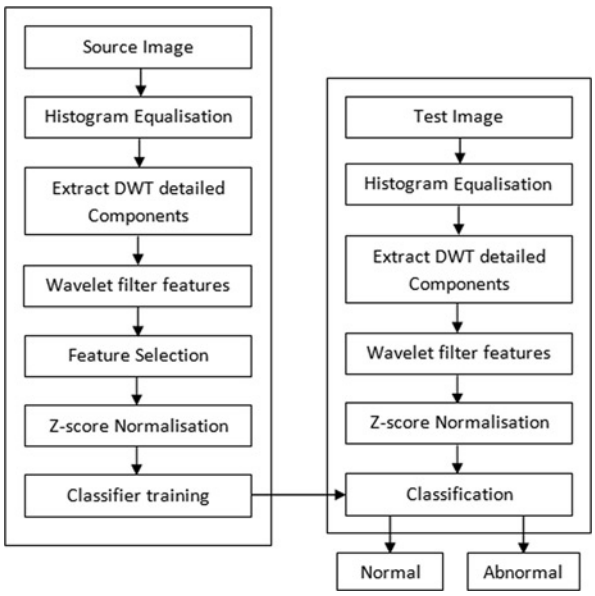

Fig. 4 *Flow diagram of disease classification*

4.1 Preprocessing of images

The biomedical images used in this work are obtained from different subjects which vary in size shape and orientation for the three different diseases, and these images have varying intensity ranges with non-uniform intensity distribution. To have a uniform distribution of intensities, the images are preprocessed by subjecting them to the standard histogram equalisation. It is also referred as the histogram linearisation process, in an image enhancement method. This process is used because it sets the intensity values of each pixel in the input image to obtain an output image which has a uniform intensity distribution along with the increase in the dynamic range of the histogram of an image. In general, the histogram equalisation process performs a transformation mapping function, T on the input intensity level r_k to produce a corresponding pixel with intensity level s_k in the output image by the following equation:

$$s_k = T(r_k) = \sum_{j=0}^{k} p_r(r_j) = \sum_{j=0}^{k} \frac{n_j}{n} \tag{1}$$

where $k = 0, 1, 2, \ldots, L-1$ and L is the number of grey-scale levels. This transformation or mapping process is called as histogram equalisation.

4.2 Discrete wavelet transform

A two-dimensional (2D) DWT applied to an image will primarily produce four different sub-bands LL, LH, HL and HH, respectively. The sub-band coding is performed by analysing the image using low-pass and high-pass filters that produce the approximation and detail coefficients in three different orientations. In Fig. 5, the one-level decomposition structure is illustrated for an input image I of size $M \times N$, $g[n]$ and $h[n]$ are the low-pass and high-pass filters, respectively, and A is the approximation coefficient of the LL sub-band and D is the detail coefficients consisting of LH, HL and HH sub-bands obtained on one-level DWT decomposition of the image. The first level decomposition structure of an image of size $M \times N$ would result in four coefficient matrices/sublimates A1, Dh1, Dv1, Dd1 each of size $M/2 \times N/2$ resolution and preserved scale. The detail components which are the high-frequency image components are extracted as they contain the desired information, which have the abrupt changes in its texture of an image which indicates the presence of the abnormal biological tissues [23]. Indeed, the detail image components extracted for further analysis are Dh1, Dv1 and Dd1 corresponding to the LH, HL and HH bands, respectively. In the proposed work, the two well-known wavelet family filters Daubechies and reverse bi-orthogonal filters are used for the feature extraction. Daubechies wavelet has a set of orthogonal scaling function and balanced frequency response. These wavelets are useful in compression and noise removal of non-linear signal processing because of its property of overlapping windows and the high-frequency coefficient spectrum of it reflect all high-frequency changes. The general characteristic of rbio is that it is non-complex and is compactly supported biorthogonal spline wavelet for which symmetry and exact reconstruction are possible. The rbio wavelet is employed to enhance image for obtaining the detail coefficients which are high-frequency components which contain the desired information for the proposed work. For the mammogram and skin feature extraction db3 and rbio3.3 wavelet filters are used while db3 and rbio3.7 are used for retinal feature extraction.

4.3 Wavelet-based filter features

The wavelet filter features are extracted from the three detailed wavelet coefficient matrices that use the statistical measures. We employed averaging as a statistical method to determine single-valued number as a typical feature to decrease the computation. The average and energy features for the vertical detail component are defined by (2) and (3), and the same are applicable for horizontal and diagonal components. The intensity-based texture features comprising of average and energy signatures of the biomedical image are used for characterising the malignancy in the biological

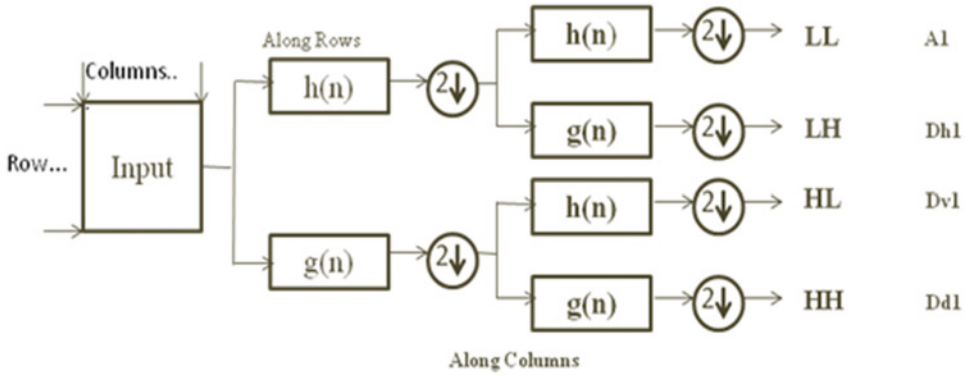

Fig. 5 *One-level DWT decomposition*

tissues

$$\text{Average Dv1} = \frac{1}{p*q}\sum_{x=1}^{p}\sum_{y=1}^{q}\left|\text{Dv1}(x,y)\right| \tag{2}$$

$$\text{Energy Dv1} = \frac{1}{p^2 * q^2}\sum_{x=1}^{p}\sum_{y=1}^{q}\left(\text{Dv1}(x,y)\right)^2 \tag{3}$$

4.4 P-*method*

In the proposed work, two group of texture features extracted comprises of six average and energy features each from the wavelet transformed biomedical images (for both normal and abnormal cases) using the two Daubechies and reverse bi-orthogonal wavelet family filters. Among them, a few number of features are chosen for each disease out of 12 features by using the *p*-value method, as they were clinically significant. For mammograms, a total of seven features were selected and for skin and retina, a total of six were chosen for each. *P*-value method is a non-traditional statistical method used for hypothesis testing by comparing the two sample averages (in this case the normal and glaucomatous eyes). In general, a *p*-value can be measured by taking the probability of the difference between the two means values. The statistical hypothesis is as follows

$$H_0\colon \mu_1 - \mu_2 = 0 \tag{4a}$$

$$H_a\colon \mu_1 - \mu_2 \neq 0 \tag{4b}$$

where H_0 is the null hypothesis which is the mean of the normal samples and is same as the mean of the abnormal samples and H_a is the alternative hypothesis which is the mean of the normal samples and is different than the mean of the abnormal samples. μ_1 and μ_2 are the means of normal and abnormal samples. Here, abnormal samples are cancerous samples for mammograms, malignant melanoma samples for skin and glaucoma samples for retina. A two-sample student's *t*-test is used to calculate the test statistics using (5) to estimate whether the mean value of each of the average and energy features has significant difference between the two classes, as

$$t\text{-stat} = \frac{\bar{x}_1 - \bar{x}_2}{\sqrt{\text{Sd}_p^2\left((1/n_1) + (1/n_2)\right)}} \tag{5}$$

where $\bar{x}_1$ and $\bar{x}_2$ are the means of the each class sample and n_1 and n_2 are the sample sizes.

sd_p is the pool variance given as follows with sd_1 and sd_2 are the variances of the classes

$$\text{Sd}_p^2 = \frac{(n_1 - 1)\text{sd}_1^2 - (n_2 - 1)\text{sd}_2^2}{n_1 + n_2 - 2} \tag{6}$$

Using the *t*-statistics, the *p*-value is calculated for each feature which is the area under the *t*-distribution curve that past the *t*-stats and is compared with the level of significance (α), the lower the *p*-value indicates that there is a significantly greater difference between the two classes. In general, the null hypothesis is rejected, if the *p*-value is less than α, otherwise the alternate hypothesis is rejected, and the null hypothesis is true. Hence, the features which exhibit *p*-values $< \alpha$ were chosen for analysis. This method is used to assess the capability of the extracted texture features to distinguish between normal and abnormal data. The significant levels considered for the study are 0.003 for mammograms, 0.001 for skin and 0.0001 for retina diseases correspondingly a 0.3, 0.1 and 0.01% chance, respectively, of the null hypothesis being true.

4.5 *Z-score normalisation of features*

Z-score is a normalisation process used for rescaling the features, i.e. the average and energy feature into the same units. It is also called as the zero-mean normalisation or standard norm. The *Z*-score normalisation is applied on each of the selected features with the sample vector consisting of seven samples for mammograms, six samples for skin and six samples for retina are converted to zero mean and unit variance. The *Z*-scores normalisation values are defined by the following equation

$$y_{\text{new}} = \frac{y_{\text{old}} - m}{\text{Sd}} \tag{7}$$

where y_{old} is the original value in the vector and y_{new} is the new value, and the *m* and *Sd* are the mean and standard deviation of the original data range, respectively.

4.6 *Classification*

4.6.1 Feed-forward neural network: A neural network is a machine-learning approach modelled from the human brain. It is an information processing system consisting of neurons as the basic building blocks which are used to construct complicated networks for any type of arbitrary function for which any analytical or statistical solutions does not exists. These neurons are highly interconnected elementary processing devices which process the information. An artificial neural network is characterised by network architecture (connection between neurons), training or learning algorithm (determining and modifying the weights on the links) and activation function (for a response of the neuron). A network structure is having no feedback loop, only a forward flow of information is called a feed-forward network. One of the most widely preferred is a multi-layered feed-forward network with back propagation shown in Fig. 6, as a single artificial neuron cannot model well for classifications that are non-linearly separable (unless the input is transformed into a better representation).

In our case, the features which are extracted are non-linear and are to be classified, so multi-layered NN is employed. The multi-layered FFNN net architecture consists of an input layer, hidden layer of any number and an output layer. The hidden layers will compute the input representation and makes the problem more linearly separable.

The multi-layer feed-forward network uses back propagation rule as training algorithm. This algorithm has four stages, viz. weights initialisation, feed-forward, back propagation of error and weights updation stages. The random values for the weights are initialised and the input signals are transmitted from input, to hidden and output layer such that a response is formed for the whole network for the inputted pattern which makes a particular prediction for performing the classification which tries to predict the class to which the input belongs. The equations for the process are as follows:

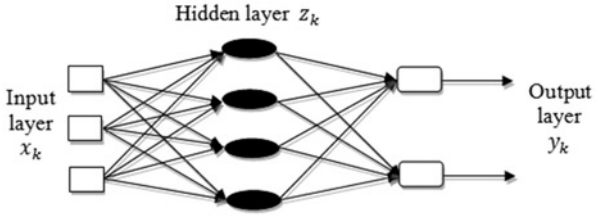

Fig. 6 *Multi-layered feed-forward network architecture*

doi: 10.1049/joe.2016.0171

Neuron pre-activation

$$a_k = \sum_i w_{ik} + w_{0k} \tag{8}$$

Hidden layer activation

$$z_k = f\left(\sum_i w_{ik} x_i + w_{0k}\right) \tag{9}$$

Output layer activation

$$\begin{aligned} y_j &= f\left(\sum_k w_{kj} z_k + w_{0j}\right) \\ &= f\left(\sum_k w_{kj}\left(f\left(\sum_i w_{ik} x_i + w_{0k}\right)\right) + w_{0j}\right) \end{aligned} \tag{10}$$

where z_k is the hidden layer output, y_j is the output, $\boldsymbol{w}$ is the weight vector and f is the activation function. These errors in the output units are fed backward through the network after each training, and the NN weights are adjusted to minimize the total mean square error.

Squared error is calculated using the delta rule and activation. During the training phase only, the backward links exist and the weight vectors are formed by the iterative flow of the training data where the network learns how to identify particular classes by knowing the characteristics of the input data. Finally, the activation function used is a linear sigmoid function, in which the output is given by equation (11)

$$y = f(x) = \frac{1}{1 + e^{-x}} \tag{11}$$

Using the sigmoid activation function binary classification can be performed as it will squash the neurons pre-activation between 0 and 1, i.e. all the output values will be between 0 and 1, such that the neuron will always be positive bounded and is strictly increasing. Once the system is optimised by training with the input pattern to obtain the trained features, the test images can be given which follow the same procedure, except the backward links, for detection of the image class, i.e. abnormal or normal images can be achieved. Here, a binary classification is taken in general, where the input features are categorised as either 0 or 1.

4.6.2 Support vector machine: SVM is a statistical learning method for both classification and regression analysis. It is a widest street approach, where it performs classification by effectively constructing a hyperplane which separates the data samples of the two classes. It produces the optimal hyperplane by maximising the margin between the two nearest samples of the both the classes, called support vectors/instances, as shown in Fig. 7. SVM classifier achieves high generalised performance as it resists to the over-fitting problem. SVM classifier overcomes the limitation of local optimisation that occurs in the neural network training and also gives unique and global optimal solution.

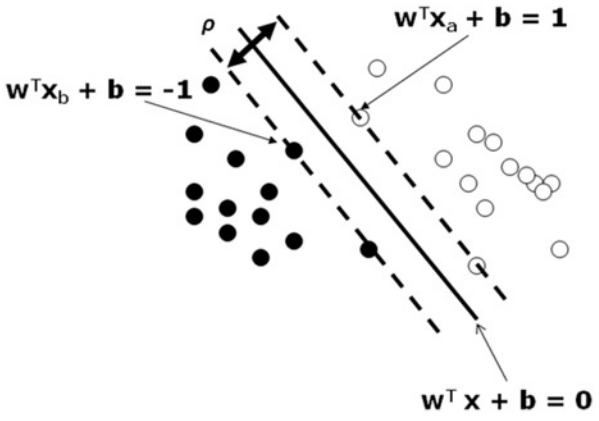

Fig. 7 *Hyperplane decision boundaries*

For a training set of data D, such that $D = (x_i, y_i)$, $i = 1, 2, 3 \ldots n$ where x_i is the sample data point belonging to both the classes and y_i is the class identifier which can be either +1 or −1. In order to get optimal hyperplane which classifies the data samples thoroughly, the width of the margin should be maximised by minimising the weight vector which is subjected to the decision boundary constraint. This constrained optimisation can be solved by introducing the Lagrange's multiplier, α and Karush–Kuhn–Tucker theorem, so the obtained weight vector is the linear sum of the input vectors, $\boldsymbol{x}_i$

$$\bar{w} = \sum_i \alpha_i y_i \bar{x}_i \tag{12}$$

Using the optimised weight vector solution, the binary classification function for linear separable data is shown in (14), for an unknown data sample vector, $\bar{\boldsymbol{x}}$. The vectors $\boldsymbol{x}_i$ with non-zero α_i are the support vectors

$$f(x) = \sum_i \alpha_i y_i \bar{x}_i \cdot \bar{\boldsymbol{x}} + b \tag{13}$$

For non-linear separable cases the data samples are transformed into other space, using the transformation function, Φ, to make the problem into linear. As the maximisation depends only on the dot product, the kernel function is the inner product of the samples in the transformed space which is given by equation (14)

$$K\left(\bar{x}_i, \bar{x}_j\right) = \Phi\left(\bar{x}_i\right) \cdot \Phi\left(\bar{x}_j\right) \tag{14}$$

The classifying function for the non-linear separable case of the SVM classifier is given by equation (15)

$$f(x) = \sum_i \alpha_i y_i K\left(\bar{x}_i, \bar{x}\right) + b \tag{15}$$

The kernels are applied to linearly non-separable problem to make linearly separable. These are used for mapping data into better representational space such that they usually determine the shape of the hyperplane. The common type of kernels are linear, Gaussian or radial basis function, polynomial and sigmoidal kernel. In this study, the Gaussian kernel is used which is considered as an optimal kernel as the features used for classification have high similarity, it gives an effective solution and is given as

$$K\left(\bar{x}_i, \bar{x}_j\right) = \exp\left(-\left\|\bar{x}_i - \bar{x}_j\right\| / 2\sigma^2\right) \tag{16}$$

SVM is the non-parametric approach where the kernel transformation is implicit and the transformation function definition is not required. The advantage of using SVM is that non-linear data can be classified with less misclassification rate, as SVM performs well for high-dimensionality and infinite, irregularly distributed or incomplete datasets. It is robust and flexible system producing a unique and optimal solution for the appropriate choice of the kernel. In this study, the binary classification of normal and abnormal biomedical images is taken which has non-linear separable features that are made separable by using the Gaussian

doi: 10.1049/joe.2016.0171

Table 1 Confusion matrix

Class label	Predicted class label	
	Normal	Abnormal
normal	TN – true negative	FN – false negative
abnormal	FP – false positive	TP – true positive

kernel and classifies the images into either +1 or −1 classes, respectively.

5 Performance metrics

The performance of a classifier can be evaluated using several criteria, which are calculated using the classification metrics or performance metrics. These metrics include confusion matrix, sensitivity, specificity, precision and accuracy. In this work, a binary classification is performed to classify the abnormal and normal images into either class '0'(positive) and class '1' (negative) class labels, respectively. For a binary classification, a 2×2 confusion matrix is obtained, whose rows indicate the class labels and the columns indicate the predicted class. Thus, a confusion matrix is used for analysing the performance of classifier which gives the prediction results, by identifying the test sample of different classes correctly or incorrectly. The four entries in the 2×2 confusion matrix shown in Table 1 correspond to the number of samples predicted by the classifier, which are the four possible conditions which are used for calculating the performance metrics, they are: true positive (TP – abnormal is diagnosed as abnormal), false positive (FP – abnormal is diagnosed as normal), true negative (TN – normal is diagnosed as normal) and false negative (FN – normal is diagnosed as abnormal).

The other performance metrics which provide a single valued information from the above-mentioned confusion matrix is used for the comparison of performance of different classifiers. These are given below.

Sensitivity: It is referred as the true positive rate (TPR), which measures the number of positives which are identified correctly

$$\mathrm{TPR} = \frac{\mathrm{TP}}{(\mathrm{TP} + \mathrm{FN})} \tag{17}$$

Specificity: It is referred as the true negative rate (TNR), which measures the number of negatives which are identified correctly

$$\mathrm{TNR} = \frac{\mathrm{TN}}{(\mathrm{TN} + \mathrm{FP})} \tag{18}$$

Precision: It is referred as the positive predictive value (PPV), which measures the number of positive samples predicted by the classifier is declared as a positive class

$$\mathrm{PPV} = \frac{\mathrm{TP}}{(\mathrm{TP} + \mathrm{FP})} \tag{19}$$

Accuracy: It is the measure of a correct prediction made by the classifier. Thus, it gives the ability of performance of the whole

Table 2 Wavelet features and corresponding *P*-value for retina

Features	Normal	Glaucoma	*P*-values
db3 (Dh_Average)	6.6415 ± 0.8642	$4.3.088 \pm 1.0183$	<0.0001
db3 (Dh_Energy)	$0.0008 \pm 0.1758 \times 10^{-3}$	$0.3620 \times 10^{-3} \pm 0.1493 \times 10^{-3}$	<0.0001
db3 (Dd_Energy)	$0.0001 \pm 0.0383 \times 10^{-3}$	$0.0741 \times 10^{-3} \pm 0.0345 \times 10^{-3}$	<0.0001
rbio3.7 (Dh_Average)	9.4660 ± 1.2445	6.0005 ± 1.4257	<0.0001
rbio3.7 (Dh_Energy)	$0.0015 \pm 0.3525 \times 10^{-3}$	$0.7278 \times 10^{-3} \pm 0.3145 \times 10^{-3}$	<0.0001
rbio3.7 (Dd_Energy)	$0.0008 \pm 0.1958 \times 10^{-3}$	$0.4031 \times 10^{-3} \pm 0.1886 \times 10^{-3}$	<0.0001

Table 3 Wavelet features and corresponding *P*-value for breast cancer

Features	Normal	Abnormal	*P*-values
db3 (Dh_Average)	2.6697 ± 0.9092	4.9747 ± 2.5746	<0.003
db3 (Dv_Average)	1.6833 ± 0.6058	3.0609 ± 1.4739	<0.003
db3 (Dv_Energy)	$2.1683 \times 10^{-4} \pm 1.6093 \times 10^{-4}$	$6.0278 \times 10^{-4} \pm 4.0829 \times 10^{-4}$	<0.003
db3 (Dd_Energy)	$6.7267 \times 10^{-5} \pm 4.9047 \times 10^{-5}$	$2.3026 \times 10^{-4} \pm 1.7465 \times 10^{-4}$	<0.003
rbio3.3 (Dv_Average)	2.8046 ± 1.0301	4.9990 ± 2.3319	<0.003
rbio3.3 (Dd_Average)	2.9858 ± 1.0620	5.6855 ± 2.9095	<0.003
rbio3.3 (Dd_Energy)	$6.4129 \times 10^{-4} \pm 5.1072 \times 10^{-4}$	0.0022 ± 0.0016	<0.003

Table 4 Wavelet features and corresponding *P*-value for skin cancer

Features	Non-melanoma	Malignant-melanoma	*P*-values
db3 (Dv_Average)	2.0389 ± 0.7564	$7.1446 \pm 3.83.03$	<0.001
db3 (Dv_Energy)	$6.1544 \times 10^{-5} \pm 5.9356 \times 10^{-5}$	$7.6420 \times 10^{-4} \pm 6.5414 \times 10^{-4}$	<0.001
rbio3.3 (Dh_Average)	2.3448 ± 1.1289	10.0409 ± 6.9411	<0.001
rbio3.3 (Dv_Average)	3.5213 ± 1.51971	12.8438 ± 6.4391	<0.001
rbio3.3 (Dd_Average)	1.9186 ± 0.7673	7.2031 ± 5.3102	<0.001
rbio3.3 (Dv_Energy)	$2.1351 \times 10^{-4} \pm 2.2504 \times 10^{-4}$	0.0023 ± 0.0018	<0.001

Table 5 Comparison of five and two filter combinations for glaucoma

Filter combination	Classifiers	TP	FP	TN	FN	TPR, %	SPC, %	PPV, %	ACC, %
five filters	FFNN	14	1	15	0	100	93.75	93.33	96.67
five filters	SVM	15	0	15	0	100	100	100	100
two filters	FFNN	14	1	15	0	100	93.75	93.33	96.67
two filters	SVM	15	0	15	0	100	100	100	100

Table 6 Performance metrics comparison for SVM and FFNN networks

Dataset	Classifiers	TP	FP	TN	FN	TPR, %	SPC, %	PPV, %
mammograms	FFNN	44	6	38	12	78.57	86.36	88
mammograms	SVM	43	7	49	1	97.72	87.5	86
retina	FFNN	47	3	49	1	97.92	94.23	94
retina	SVM	50	0	50	0	100	100	100
skin	FFNN	42	8	38	12	77.78	82.61	84
skin	SVM	45	5	44	6	88.24	89.8	90

Table 7 Accuracy comparison of SVM and FFNN classifiers

Dataset	SVM classifier accuracy	FFNN classifier accuracy
mammograms	92	82
retina	100	96
skin	89	80

Table 8 Computational complexity comparison for 2D signal (image)

Filter combination	Computational complexity		
	Product (P)	Addition (S)	Total No. of operations
five filters	72	52	124
two filters	32	24	56

Fig. 8 *Main GUI for multiple disease diagnosis*

Fig. 9 *Classification results for the whole dataset along with accuracy for both the classifiers*
a Mammograms
b Retina
c Skin

doi: 10.1049/joe.2016.0171

classifier

$$\mathrm{ACC} = \frac{(\mathrm{TP} + \mathrm{TN})}{(\mathrm{TP} + \mathrm{FP} + \mathrm{TN} + \mathrm{FN})} \tag{20}$$

6 Results and analysis

In the earlier research work, the disease classification is done based on three wavelet family filters with five filters (db3, sym3, rbio3.3, rbio3.5 and rbio3.7) [10, 24]. In the proposed research work, the computational complexity of the disease classification is reduced by using only two wavelet family filters, for the diagnosis of retinal disease, like glaucoma. The two filters db3 and rbio3.7 are used for feature extraction which are retaining the same accuracy as that of five filters. Also, the multiple disease classification like breast cancer and skin cancer is done. It is observed that for both the breast cancer and skin cancer the combination of two wavelet filters db3 and rbio3.3 are more effective. Thus, for a mammogram seven wavelet features, for skin and retina, a set of six wavelet features of each are selected based on their respective *p*-values from each image in the dataset. The selected features for each of the disease case for glaucoma, breast cancer and skin cancer are tabulated in Tables 2–4, respectively.

These selected feature vectors are then fed to the FFNN and SVM classifiers to classify the normal and abnormal images, where the classification for the similar dataset and a single test image are done by undergoing the same procedures followed before the training phase. Then, the obtained test values are compared with the trained set of feature values for classification. It is observed that though the number of filters are reduced, the same accuracy is maintained for both SVM and FFNN classifiers for glaucoma classification as shown in Table 5.

In the proposed work, the two filter combinations are extended to the other two datasets of mammograms and skin cancer. The effectiveness of SVM classification is analysed by evaluating the performance metrics, which are compared with FFNN networks for each dataset of 100 images that are tabulated in Table 6.

The overall accuracy for each of the network is calculated by using the confusion matrices for all the three datasets shown in Table 7, and it is clear that the SVM is showing better performance than FFNN.

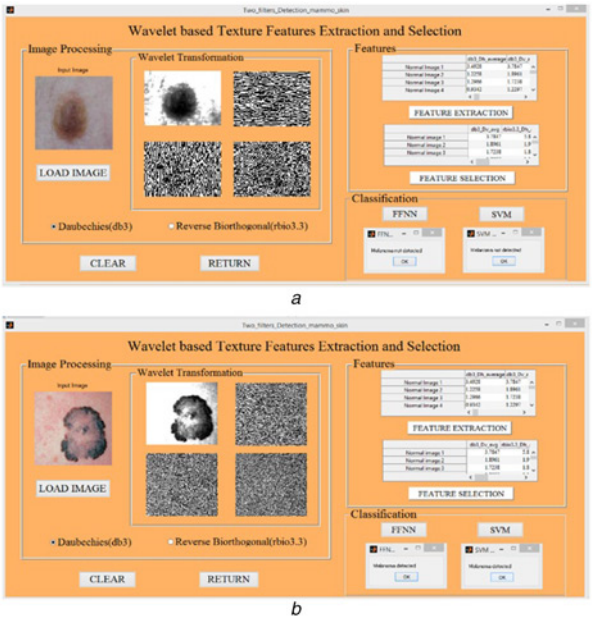

Fig. 11 *Classifier results for skin cancer*
a Normal image
b Abnormal image

The implemented method has the advantage of reducing the computational complexity as the numbers of wavelet filters are reduced. The daubechies, symlet and reverse bi-orthogonal wavelet family filters are all bi-orthogonal filters with high-pass and low-pass filter taps of lengths T1 and T2. The required number of summations (S) and multiplications (P) are calculated [25] as the following equations

$$P = T_1 + T_2 \tag{21}$$

$$S = T_1 + T_2 - 2 \tag{22}$$

The computational complexity in general case can be computed as

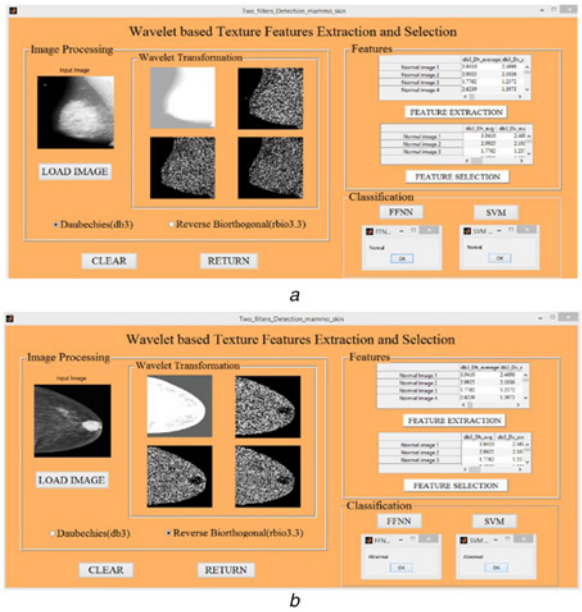

Fig. 10 *Classifier results for breast cancer*
a Normal image
b Abnormal image

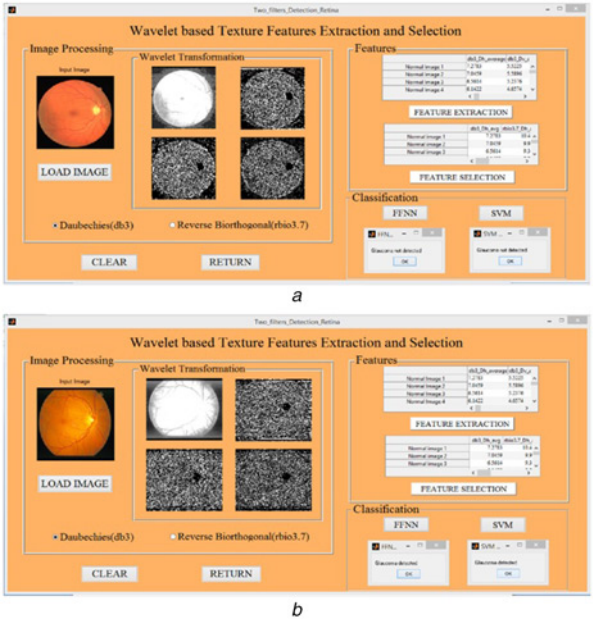

Fig. 12 *Classifier results for glaucoma*
a Normal image
b Abnormal image

the number of the required floating point operations per sample of the 1D signal, per scale. For 2D signals, the image with separable filtering we need to multiply the above equations by two to account for horizontal and vertical filtering, and then the computational complexity is depicted in Table 8.

The proposed method is implemented in MATLAB, by creating a GUI for classification of the whole dataset and detection of disease for a single test image for all of the three datasets. Multiple disease diagnosis GUI as shown in Fig. 8 consists of classification and test image detection option for each of the diseases. The classification GUI presented in Figs. 9*a–c* provides the accuracy of the neural networks and support vector machine for breast cancer, retina and skin cancer. In the classification panel, the two classifiers are used to classify normal or abnormal image class for the given test input image from the three different datasets of mammograms, skin and retina which are shown in Figs. 10–12, respectively.

7 Conclusion

This research work presents the implementation of an efficient disease classifier using only two wavelet filters. It is observed that the two wavelet filters db3 and rbio3.3 are more efficient for the classification of skin and breast cancer diseases whereas for the glaucoma disease the wavelet filters db3 and rbio3.7 are more effective with reduced computational complexity. This implementation shows that the dependence between features extracted using two wavelet filters has been subjected to feature selection by using *P*-value method. The selected texture features are fed to both SVM and FFNNs to distinguish between normal and abnormal samples and their performance metrics are compared. The comparison proves that SVM is efficient than the FFNN neural network, with an improved accuracies of 93.33% for mammograms, 100% for retinal glaucomatous images and 90% for skin disease.

8 Acknowledgment

The authors thank the Department of ECE, JNTUK University of Engineering Viziangaram for the constant support and encouragement.

9 References

[1] Verma B., Zakos J.: 'A computer-aided diagnosis system for digital mammograms based on fuzzy-neural and feature extraction techniques', *IEEE Trans. Inf. Technol. Biomed.*, 2001, **5**, (1), pp. 46–54
[2] Korotkov K., Garcia R.: 'Computerized analysis of pigmented skin lesions: a review', *Artif. Intell. Med.*, 2012, **56**, (2), pp. 69–90
[3] Celebi M.E., Iyatomi H., Schaefer G., *ET AL.*: 'Lesion border detection in dermoscopy images', *Comput. Med. Imaging Graph.*, 2009, **33**, (2), pp. 148–153
[4] Abbas Q., Celebi M.E., Garcıa I.F.: 'Skin tumor area extractionusing an improved dynamic programming approach', *Skin Res. Technol.*, 2012, **18**, (1), pp. 133–142
[5] Dong A., Wang B.: 'Feature selection and analysis on mammogram classification'. Proc. IEEE PacificRim Conf. on Communications, Computers and Signal Processing (PACRIM '09), Victoria, BC, Canada, August 2009, pp. 731–735
[6] Tirtajaya A., Santika D.: 'Classification of microcalcificationusing dual-tree complex wavelet transform and support vector machine'. Proc. of the 2nd Int. Conf. on Advances in Computing, Control and Telecommunication Technologies (ACT '10), Jakarta, Indonesia, December 2010, pp. 164–166
[7] Moayedi F., Azimifar Z., Boostani R., *ET AL.*: 'Contourlet-based mammography mass classification using the SVMfamily', *Comput. Biol. Med.*, 2010, **40**, (4), pp. 373–383
[8] Khademi A., Krishnan S.: 'Shift-invariant discrete wavelet transform analysis for retinal image classification', *Med. Biol. Eng. Comput.*, 2007, **45**, (12), pp. 1211–1222
[9] Lee N., Laine A.F., Smith T.R.: 'Learning non-homogenous textures and the unlearning problem with application to drusen detection in retinal images'. Proc. fifth IEEE Int. Symp. on Biomedical Imaging: From Nano toMacro (ISBI '08), Paris, France, May 2008, pp. 1215–1218
[10] Summeet D., Rajendra Acharya U., Chowriappa P., *ET AL.*: 'Wavelet-based energy features for glucomatous image classification', *IEEE Trans. Inf. Technol. Biomed.*, 2012, **16**, (2), pp. 121–142
[11] Weiss S., Kulikowski C.A., Saflr A.: 'Glaucoma consultation by computer', *Comput. Biol. Med.*, 1998, **8**, (1), pp. 24–40
[12] Weiss S., Kulikowski C.A., Amarel S.: 'A model-based method for computer-aided medical decision-making', *Artif. Intell.*, 1978, **11**, (2), pp. 145–172
[13] Acharya U.R., Dua S., Du X., *ET AL.*: 'Automated diagnosis of glaucoma using texture and higher order spectra features', *IEEE Trans. Inf. Technol. Biomed.*, 2011, **15**, (3), pp. 449–455
[14] Maglogiannis I.G., Zafiropoulos E.P.: 'Characterization of digital medical images utilizing support vector machines', *BMC Med. Inf. Decis. Mak.*, 2004, **4**, (2), pp. 1–8
[15] Manousaki G., Manios A.G., Tsompanaki E.I., *ET AL.*: 'A simple digital image processing system to aid in melanoma diagnosis in an everyday melanocytic skin lesion unit: a preliminary report', *Int. J. Dermatol.*, 2006, **45**, (3), pp. 402–410
[16] Goppner D., Muller J., Kruger S., *ET AL.*: 'High incidence of naevi-associated BRAF wild-type melanomaand dysplastic naevi under treatment with the class I BRAF inhibitor vemurafenib', *Acta Derm. Venereol.*, 2014, **94**, (5), pp. 517–520
[17] Maglogiannis I., Doukas C.N.: 'Overview of advanced computer vision systems for skin lesions characterization', *IEEE Trans. Inf. Technol. Biomed.*, 2009, **13**, (5), pp. 721–733
[18] 'Digital Mammography'. Available at http://marathon.csee.usf.edu/Mammography/Database.html, accessed 15 November 2015
[19] 'DataBase'. Available at http://www.isi.uu.nl/Research/Databases/DRIVE/download.php, accessed 31 January 2016
[20] 'Structured Analysis of the Retina'. Available at http://www.ces.clemson.edu/ahoover/stare/, accessed 1 February 2016
[21] 'Clinical Dermatology'. Available at http://www.danderm-pdv.is.kkh.dk/atlas/index.html, accessed 12 November 2015
[22] 'The dermatology resource'. Available at http://www.dermnetnz.org/, accessed 25 October 2015
[23] Jamarani S.M.H., Rezai-rad G., Behnam H.: 'A novel method for breast cancer prognosis using wavelet packet based neural network'. Proc. 27th Annual Int. Conf. of the Engineering in Medicine and Biology Society (IEEE-EMBS '05), Shanghai, China, September 2005, pp. 3414–3417
[24] Simon N., Hymavathy K.P.: 'Early stage glaucoma screening and segmentation using FFNN', *Int. J. Eng. Res. Technol.*, 2015, **4**, (4), pp. 17–28
[25] Polyak N., Pearlman W.A.: 'A new flexible biorthogonal filter design for multiresolution filterbanks with application to image compression', *IEEE Trans. Signal Process.*, 2000, **48**, (8), pp. 2279–2288